**19.0    MECHANISM OF DWELL FATIGUE CRACK INITIATION IN TI-7AL UNDER BIAXIAL TENSION-TENSION LOADS**

Garrison Hommer (CSM)
Faculty: Aaron Stebner (CSM) and Peter Collins (ISU)
Industrial Mentor: Adam Pilchak (AFRL)

**19.1    Project Overview and Industrial Relevance**

Stress dwell periods and constant high mean stresses are detrimental to fatigue life of alpha phase (HCP) dominated Ti alloys at low temperatures, less than approximately 200° C. Limited deformation mechanisms of HCP crystal structure are responsible for this effect. This effect is even more pronounced in alloys containing greater than 5 weight percent aluminum, as this has been shown to suppress twinning [19.1], further limiting deformation mechanisms. Strong slip system anisotropy, by a factor of up to 3.33 for critical resolved shear stress (CRSS), gives rise to plastically hard and soft grains [19.2]. This effect is not seen at higher temperatures as the CRSS anisotropy is reduced.

Soft grains, relative to their stress tensor, are preferentially oriented to slip, whereas hard grains are not. Limited deformation mechanisms reduce material hardening, causing room temperature creep in soft grains. When a soft grain is positioned next to a hard grain, local load shedding and dislocation pile-up occurs at the grain boundary, as slip does not occur in the hard grain. These dislocation pile-ups cause microvoid formation, leading to crack initiation and ultimately failure. Study of this behavior is motivated by jet engine turbine compressor discs, which are typically made from titanium alloys and experience a stress dwell period during aircraft cruise. It is known that the discs experience orthogonal biaxial tension-tension stress states ranging in proportion from 1:4 in the root to 1:1 in the web. While studies of this phenomenon are extensive for uniaxial loading, they are lacking for biaxial. The project goal is to understand this phenomenon under tension-tension biaxial loads to aid in design and life prediction of jet engine turbine compressor discs.

**19.2    Previous Work**

Prior to project initiation, an experimental setup was conceived for planar biaxial *in situ* loading experiments. A planar biaxial load frame was designed for use at the 1-ID beamline of the Advanced Photon Source (APS) at Argonne National Lab [19.3], such that it could be rotated 360° in the beam. Serial reconstruction of 2D diffraction patterns captured every 0.1° for each load step give 3D data that includes for each grain: center of mass, volume, phase, orientation, deformation gradient, and average lattice strain [19.4]. This technique is referred to as far-field high energy diffraction microscopy (ff-HEDM). ff-HEDM allows grain neighborhood orientation effects to be investigated in relation to dwell fatigue and provides experimental data for model validation and development. Stereo digital image correlation (DIC) during loading provides surface strains of specimen gage. Cruciform specimen geometries were designed for diffraction capability, as well as tension-tension, tension-compression, and compression-compression loading [19.3, 19.5]. Variable maximum gage stress relative to fixed applied load allows specimen optimization for a wide range of material strengths. Specimen geometries are shown in **Fig. 19.1** and the experimental setup at the APS is shown in **Fig. 19.2**.

*In situ* dwell fatigue experiments have been conducted at APS for X:Y gage stress ratios of 1:1 (also referred to as 4:4), 1:2, and 1:4. *In situ* monotonic loading to failure experiments have been conducted for X:Y gage stress ratios of 1:1 and 1:2. For the first round of dwell fatigue experiments ff-HEDM data points were collected at unloaded states for reference and after dwell cycles 1-10, 50 and 100. Dwell cycling was done with 1 s loading and unloading to 80% yield stress with 120 s dwell periods under force control. The second round of dwell fatigue experiments included 1:1 and 1:4 X:Y gage stress ratios. As additional virgin specimens were unavailable, specimens used for previous 1:1 and 1:4 dwell fatigues tests were used. Ramp times of 1 s were maintained, but dwell stress was increased to 100% of yield stress as opposed to 80%. This was for the purpose of accelerating mechanisms responsible for dwell fatigue. The ff-HEDM data points were collected at loaded and unload states. A dwell time of at least 120 s took place before data collection at load began. Collecting data at load also meant that the total dwell time for each cycle included data collection time of approximately 25 minutes, in addition to the initial 120 s dwell. However, dwell time of 120 s has been shown to produce near maximum dwell debit. Additional time of collecting these data required cycle reduction from 0 – 10, 50 and 100 to 0 – 5 and 50.

### 19.3    Recent Progress

A PhD thesis on the work of this project has been written and was successfully defended on March 20, 2018. The following sections summarize some of the thesis content that has not been previously discussed.

#### 19.3.1    Normalized Resolved Shear Stress Pole Figures

A method for bounding tensor-based resolved shear stress calculations by [0, 0.5] using normalized multiaxial stress tensors, allowing interpretation analogous to Schmid factors was devised. A method to visualize orientation dependence of slip system activity resulting from these calculations using pole figures was also devised. Examples of these normalized resolved shear stress (nRSS) pole figures (PFs) are shown in **Fig. 19.3** for a composite of the basal and prismatic slip systems and X:Y stress ratios of 1:1 and 1:4.

#### 19.3.2    Stress Coaxiality Angle as a Plasticity Metric

Stress coaxiality angle (SCA) and was used as an indicator of plastic deformation. The SCA is defined as

$$\varphi = cos^{-1}\left(\frac{\boldsymbol{\sigma}_{applied} : \boldsymbol{\sigma}_{grain}}{\|\boldsymbol{\sigma}_{applied}\|\|\boldsymbol{\sigma}_{grain}\|}\right)$$

where $\boldsymbol{\sigma}_{applied}$ is the applied stress tensor ($\boldsymbol{\sigma}_{11} = \boldsymbol{\sigma}_{22} = 1$ and all other components equal to 0 for the 4:4 stress ratio specimen, and $\boldsymbol{\sigma}_{11} = 1, \boldsymbol{\sigma}_{22} = 4$, and all other components equal to 0 for the 1:4 stress ratio specimen) and $\boldsymbol{\sigma}_{grain}$ is the measured grain stress tensor. Stress coaxiality angle is a scalar measure of the alignment between two stress states and in the case of the form given, the alignment between the macroscopic (i.e. applied) stress and the stress state of a grain. The SCA has been shown to be relatively low (~5-10°) and constant during elastic deformation and begin to increase at the onset of plastic deformation with continued increase as plastic deformation proceeds [19.6]. Intuitively it makes sense that SCA increases as plastic deformation proceeds because components of the grain stress tensor that are most resolved on an active slip system are relieved while other components are not, therefore causing the grain stress tensor to deviate from the applied stress tensor.

#### 19.3.3    Cyclic Evolution of Trends in Grain Orientations and Stress Metrics

The SCA for the 4:4 and 1:4 stress ratio specimens at cycles 1 and 50 are plotted as empirical cumulative distribution functions (ECDF) in **Fig. 19.4**. An ECDF gives the probability that a variable exists within a certain range of values. For example, the ECDF for 1:4 Stress, Cycle 1 indicates there is approximately a 40% chance (i.e. 0.4 Fraction of Data) the SCA of a grain is less than 18° and conversely, a 60% chance it is greater than 18°, with 20° corresponding to the median of the data set (i.e. 0.5 Fraction of Data). The 1:4 specimen has a median SCA of 20.4° and the 4:4 specimen of 12.4°, which corresponds to only about 5% of the 1:4 ECDF. This higher median SCA combined with the similar but shifted ECDFs of the two specimens indicates increased plastic deformation in the 1:4 specimen. While the minimum SCAs are similar in all ECDFs, the 1:4 specimen contains far fewer low SCA grains than the 4:4 specimen, evidencing fewer 1:4 hard behaving grains. Insights about cyclic plastic deformation can also be made.

Both 4:4 and 1:4 stress ratio specimen ECDFs exhibit leftward shifts with the 4:4 specimen being far more substantial. Also, the 4:4 shift is more dramatic for higher SCAs. This shift indicates cyclic plasticity that is most prominent in the softest grains. The more substantial shift in the 4:4 specimen may be due to enhanced hardening in the 1:4 specimen through a mixture of basal and prismatic slip, while the 4:4 specimen deformed primarily through basal. The prismatic slip system contains three planes allowing for the creation of sessile dislocations through intersections and combinations into new dislocations that are not in slip directions, whereas the basal slip system contains 1 plane, thereby preventing this mechanism. These dislocations behaviors likely also contribute to the observed basal critical resolved shear stress (CRSS) softening. The ECDFs of RSS on basal and prismatic slip systems are plotted for the 4:4 specimen in **Fig. 19.5**. Basal CRSS softening is seen as the leftward shift of the high stress distribution portions of the ECDFs between cycles 1 and 50. The softening may also be contributed to the cyclic accumulation of soft planar slip bands through the shearing of $Ti_3Al$ nanoprecipitates. This was also observed in the 1:4 specimen.

#### 19.3.4    Interdependencies of Grains Orientations and Stress Metrics

One particular plot that provides extensive insight into soft and hard grain interactions is that of SCA vs. stress triaxiality (i.e. the ratio of hydrostatic stress to Mises stress) shown in **Fig. 19.6**. The near-singular stress triaxiality

value that occurs for the lowest SCA grains corresponds to neutrally behaving grains (i.e. not soft or hard) with stress states most similar to the macroscopic applied stress. Stress triaxiality decreases (i.e. Mises stress dominates hydrostatic stress) for hard grains receiving load from soft grains and increases (i.e. hydrostatic stress dominates Mises) for soft grains exhibiting load shedding. It is also shown that load shedding (i.e. plastic deformation) and receiving both increase SCA. Load shedding increases SCA in soft grains through the previously mentioned mechanism of slip relieving the most resolved components of the stress tensor, while load receiving increases SCA in hard grains through taking on these relieved components. This behavior provides explanation for dwell fatigue crack initiation sites being observed on softly oriented, near basal planes. The explanation being that in crack initiation grains, basal slip bands (having the lowest CRSS due to cyclic softening and limited hardening) accumulate through load shedding while stress triaxiality simultaneously increases, which promotes decohesion of the slip bands and subsequent crack initiation.

### 19.3.5   Soft and Hard Grain Neighborhood Effects

Soft grains were selected from the 4:4 specimen data set through the criterion of minimum Mises stress. The orientations of these grains are shown on the (0001) PF in **Fig. 19.7** and generally represent soft basal orientations. Their SCA behavior as a function of their neighborhood prismatic nRSS is shown in **Fig. 19.8**. Their SCA is seen to increase with increasing neighborhood prismatic nRSS, indicating that softer neighborhoods lead to increased SCA in soft grains. This is due to softer neighborhoods allowing for less constrained deformation in soft grains. This is just one example of how individual grain behavior is influenced by neighborhoods.

### 19.4   Plans for Next Reporting Period

This is the final reporting period for this project. Additional work to be completed and related to this project is the publication of journal articles. Several journal articles in preparation are summarized below.

- Invited planar biaxial *in situ* far-field high energy diffraction microscopy experiment article for submission to the Journal of Experimental Mechanics

- Normalized resolved shear stress pole figure visualization method article for submission to Scripta Materialia

- Fractography of microstructure and failure surfaces in Ti-7Al subjected to tension-tension biaxial dwell fatigue and tension-tension biaxial monotonic loading

- Micromechanics of tension-tension biaxial dwell fatigue in Ti-7Al

### 19.5   References

[19.1]   J. C. Williams, R. G. Baggerly, and N. E. Paton, "Deformation behavior of HCP Ti-Al alloy single crystals," *Metall. Mater. Trans. A*, vol. 33, no. 13, pp. 837–850, 2002.

[19.2]   Z. Zhang, M. A. Cuddihy, and F. P. E. Dunne, "On rate-dependent polycrystal deformation: the temperature sensitivity of cold dwell fatigue," *Proc. R. Soc. Math. Phys. Eng. Sci.*, vol. 471, no. 2181, p. 20150214, Sep. 2015.

[19.3]   G. M. Hommer, J. S. Park, P. C. Collins, A. L. Pilchak, and A. P. Stebner, "A New In Situ Planar Biaxial Far-Field High Energy Diffraction Microscopy Experiment," in *Advancement of Optical Methods in Experimental Mechanics, Volume 3*, S. Yoshida, L. Lamberti, and C. Sciammarella, Eds. Cham: Springer International Publishing, 2017, pp. 61–70.

[19.4]   J. V. Bernier, N. R. Barton, U. Lienert, and M. P. Miller, "Far-field high-energy diffraction microscopy: a tool for intergranular orientation and strain analysis," *J. Strain Anal. Eng. Des.*, vol. 46, no. 7, pp. 527–547, Oct. 2011.

[19.5]   G. M. Hommer and A. P. Stebner, "Development of a Specimen for In-Situ Diffraction Planar Biaxial Experiments," in *Fracture, Fatigue, Failure and Damage Evolution, Volume 8*, A. M. Beese, A. T. Zehnder, and S. Xia, Eds. Cham: Springer International Publishing, 2016, pp. 45–50.

[19.6]   T. J. Turner *et al.*, "Crystal Plasticity Model Validation Using Combined High-Energy Diffraction Microscopy Data for a Ti-7Al Specimen," *Metall. Mater. Trans. A*, vol. 48, no. 2, pp. 627–647, Feb. 2017.
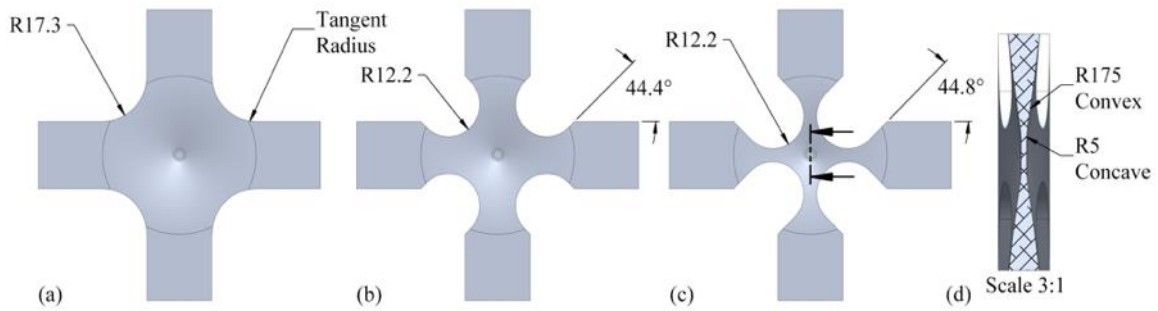
## 19.6    Figures and Tables



Figure 19.1: Three specimen geometries with maximum gage stresses of (a) 400 MPa, (b) 800 MPa, and (c) 1700 MPa, and (d) specimen cross-section.
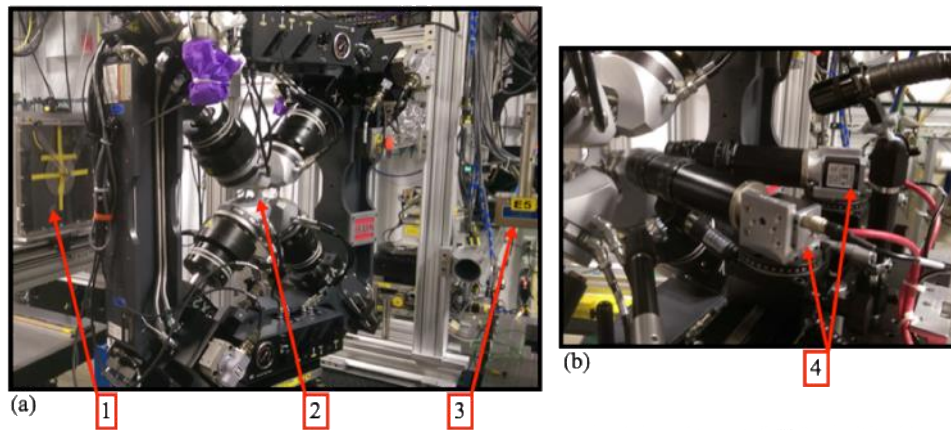


Figure 19.2: Experimental setup in the 1-ID hutch of APS at Argonne National Lab showing (1) the area detector, (2) the specimen mounted in the planar biaxial load frame, (3) the final X-ray beam collimation slits before it penetrates the sample and (4) the DIC setup in image capturing position.
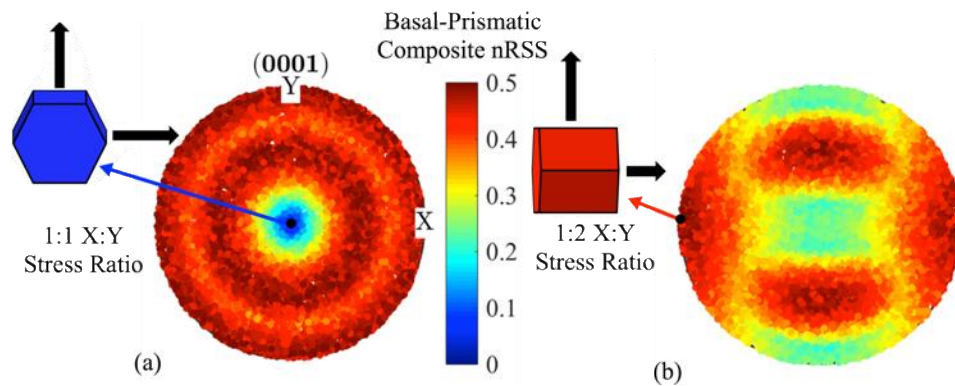


Figure 19.3: Basal-prismatic composite nRSS pole figures for (a) 1:1 and (b) 1:2 X:Y stress ratios.

19.4
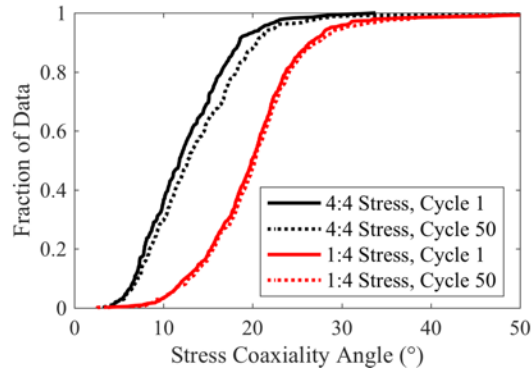
Figure 19.4: Empirical cumulative distribution functions of SCA for 4:4 and 1:4 stress ratios at cycles 1 and 50.
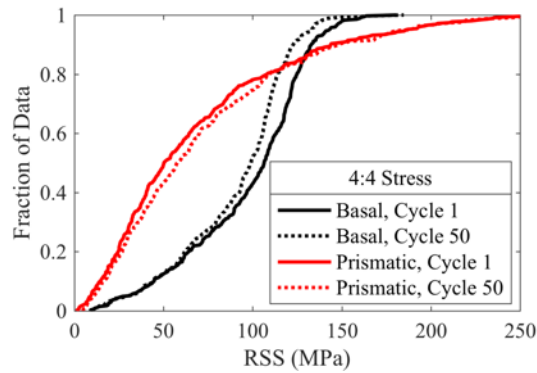


Figure 19.5: Empirical cumulative distribution functions of RSS on basal and prismatic slip systems for 4:4 stress ratio at cycles 1 and 50.
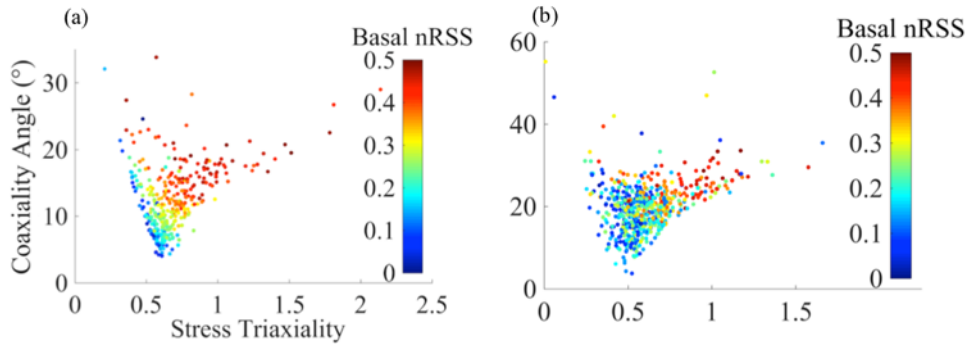


Figure 19.6: Stress coaxiality angle vs. stress triaxiality in the (a) 4:4 and (b) 1:4 stress ratio specimens colored according to their basal nRSS.
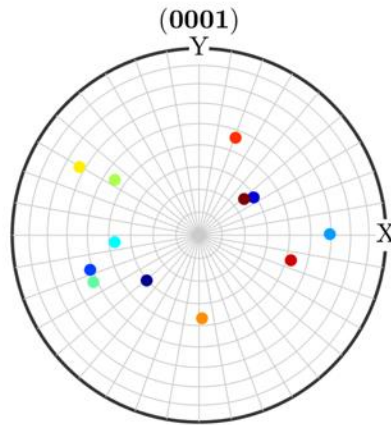
19.5

Figure 19.7: Orientations of soft grains based on minimum Mises stress plotted on (0001) equal area spherical projection PF for 4:4 stress ratio.
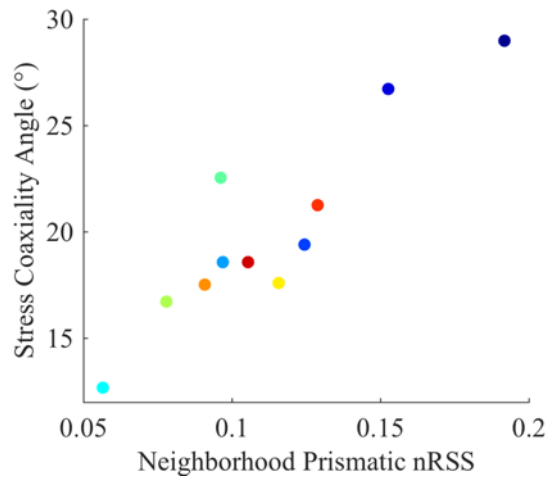


Figure 19.8: Stress coaxiality angle vs. neighborhood prismatic nRSS of soft grains based on minimum Mises stress for 4:4 stress ratio specimen.